In-Plane Anisotropy of Charge Density Wave Fluctuations in 1T-$TiSe_2$

Xuefei Guo,[1,*] Anshul Kogar,[2,†] Jans Henke,[3] Felix Flicker,[4] Fernando de Juan,[5,6] Stella X.-L. Sun,[1] Issam Khayr,[1,7] Yingying Peng,[8] Sangjun Lee,[1] Matthew J. Krogstad,[9] Stephan Rosenkranz,[9] Raymond Osborn,[9] Jacob P. C. Ruff,[10] David B. Lioi,[11] Goran Karapetrov,[11] Daniel J. Campbell,[12] Johnpierre Paglione,[12,13] Jasper van Wezel,[3] Tai C. Chiang,[1] and Peter Abbamonte[1,‡]

[1]*Department of Physics and Materials Research Laboratory, University of Illinois, Urbana, Illinois 61801, USA*
[2]*Department of Physics and Astronomy, University of California at Los Angeles, Los Angeles, California 90095, USA*
[3]*Institute for Theoretical Physics Amsterdam, University of Amsterdam, Science Park 904, 1098 XH Amsterdam, The Netherlands*
[4]*School of Physics, Tyndall Avenue, Bristol BS8 1TL, United Kingdom*
[5]*Donostia International Physics Center, P. Manuel de Lardizabal 4, 20018 Donostia-San Sebastián, Spain*
[6]*IKERBASQUE, Basque Foundation for Science, Plaza Euskadi 5, 48009 Bilbao, Spain*
[7]*School of Physics and Astronomy, University of Minnesota, Minneapolis, Minnesota 55455, USA*
[8]*International Center for Quantum Materials, School of Physics, Peking University, Beijing 100871, China*
[9]*Materials Science Division, Argonne National Laboratory, Lemont, Illinois 60439, USA*
[10]*CHESS, Cornell University, Ithaca, New York 14853, USA*
[11]*Department of Physics, Drexel University, Philadelphia, Pennsylvania 19104, USA*
[12]*Maryland Quantum Materials Center, Department of Physics, University of Maryland, College Park, Maryland 20742, USA*
[13]*Canadian Institute for Advanced Research, Toronto, Ontario M5G 1Z8, Canada*

(Received 20 January 2025; accepted 19 August 2025; published 25 September 2025)

We report measurements of anisotropic triple-q charge density wave (CDW) fluctuations in the transition metal dichalcogenide 1T-$TiSe_2$ over a large volume of reciprocal space with x-ray diffuse scattering. Above the transition temperature, T_{CDW}, the in-plane diffuse scattering is marked by ellipses which reveal that the in-plane fluctuations are anisotropic. In addition, the out-of-plane diffuse scattering is characterized by rodlike structures which indicate that the CDW fluctuations in neighboring layers are largely decoupled. Our analysis of the diffuse scattering line shapes and orientations suggests that the three charge density wave components contain independent phase fluctuations with a hierarchy of length scales, leading to intricate fluctuation patterns that go beyond the conventional 2D-to-3D crossover picture.

DOI: 10.1103/j8vm-wb65

Fluctuations are central to the critical behavior observed near continuous phase transitions [1,2]. In quasi-two-dimensional layered systems, where interplane coupling is weak, fluctuations can persist to temperatures far exceeding the transition temperature and can affect the system's normal state electronic properties. In these cases, in-plane fluctuations start to build below the mean field transition temperature T_{MF}, but they initially remain uncorrelated between layers. As the temperature is reduced further and approaches the critical temperature T_c, a 2D-to-3D crossover occurs as the interplane correlation length starts to exceed the interplane distance. At T_c, both in-plane and out-of-plane correlation lengths diverge and full three-dimensional long-range order sets in [2]. A wide variety of physical systems have been shown to conform to this simple description [2–8]; because transition metal dichalcogenides are layered compounds, and their charge density wave (CDW) order is characterized by large ratios of $2\Delta(0)/k_B T_{CDW}$, where $\Delta(0)$ is the zero-temperature gap and T_{CDW} is the charge density wave transition temperature, fluctuations in these materials should abide by a similar phenomenology.

This picture is complicated, however, in the CDW-hosting transition metal dichalcogenides by the fact that their charge order consists of three unidirectional components, in a structure that is often referred to as a triple-q CDW [see Figs. 1(d)–1(g)] [9]. The triple-q structure preserves the threefold crystallographic in-plane symmetry, despite the unidirectionality of the individual CDW components [10]. Preservation of this symmetry gives an energetic advantage to triple-q order over CDWs containing only a single component in these compounds, which can be described by an effective "attraction" between CDW components in their free energy description (see Supplemental Material [11]) [22]. For the same reason, short-range ordered regions above T_{CDW} will consist of local triple-q order, while the large value of $2\Delta(0)/k_B T_{CDW} \approx 8.7$ [23] implies that long-range phase coherence is prevented at those temperatures by the

*Contact author: xuefeig2@illinois.edu
†Contact author: anshulkogar@physics.ucla.edu
‡Contact author: abbamont@illinois.edu

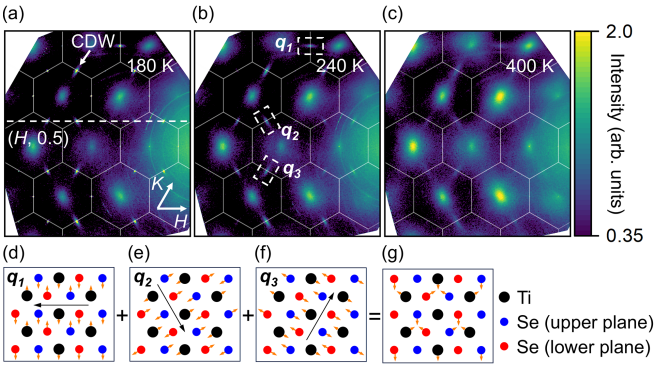

FIG. 1. In-plane anisotropy of CDW fluctuations. (a)–(c) In-plane momentum maps at $L = 0.5$ r.l.u. for temperatures below (180 K), above (240 K), and well above (400 K) $T_{\mathrm{CDW}}(=195\ \mathrm{K})$. Below T_{CDW}, sharp peaks are observed at the Brillouin zone boundaries (white line), indicating the presence of an ordered state. As the CDW is melted, CDW fluctuations become elongated along the in-plane CDW vectors q_i $(i = 1, 2, 3)$. The diffuse feature at the center of the Brillouin zone corresponds to the tail of the structural Bragg peaks from neighboring L planes. The intensity scale bar is in arbitrary units and follows a logarithmic scale. (d)–(f) Schematic depictions of the in-plane displacement pattern of the three components contributing to the triple-q CDW. (d) q_1-type component, (e) q_2-type component, and (f) q_3-type component. Black arrows indicate the direction of the propagation vector for each CDW component, while small orange vectors indicate the atomic displacement directions that would result from having only each single component present. (g) The full in-plane triple-q distortion pattern obtained by adding the atomic displacements from all three CDW components. Black circles represent Ti atoms, blue circles represent Se atoms in the upper plane, and red circles represent Se atoms in the lower plane.

proliferation of phase fluctuations rather than the suppression of the CDW amplitude [24,25]. Phase slips may occur either in all three components simultaneously, or independently in different components. As described in Supplemental Material [11], the latter option is generically favored in the free energy description for a triple-q CDW.

Because the CDW order in $1T$-$TiSe_2$ contains three components with independent phase fluctuations, both the fluctuating regions and the crossover to three-dimensional order may obtain a more structured character when compared to the usual 2D-to-3D crossover scenario. In this Letter, we show that while out-of-plane diffuse scattering indicates decoupled CDW fluctuations in neighboring layers, the in-plane diffuse scattering arising from individual CDW components is anisotropic, with a directionally dependent characteristic length scale. We argue that, in the temperature range near but above T_{CDW}, each CDW component contains independent phase slips. While the combined triple-q short-ranged order remains isotropic on average, the mean distance between phase slips for any given component is anisotropic and determines its distinct correlation length scales in different directions. We thus demonstrate that despite its threefold symmetry and quasi-two-dimensional crystal structure, $1T$-$TiSe_2$ possesses anisotropic CDW fluctuations in the basal plane and a hierarchy of three distinct length scales arising from independently fluctuating CDW components [26].

To carry out our experiments, we used two different batches of $TiSe_2$ single crystals with different synthesis methods. We synthesized vacancy-reduced $TiSe_2$ crystals using a Se-flux method under high pressure [27]. These are insulating at low temperatures; their resistivity is hysteretic from 30–80 K. We grew another batch of samples using iodine vapor transport [28,29]. These are crystallographically cleaner with less mosaicity; they are semimetallic at low temperatures with higher carrier concentrations. The electrical transport measurement shows no qualitative difference between semimetallic and insulating samples at high temperatures above T_{CDW} [27], and trace disorder is therefore expected to have minimal impact on CDW fluctuations away from T_{CDW}. Indeed, both batches of samples give identical diffuse scattering results. The data presented in the main manuscript are from the semimetallic sample, while the data for the vacancy-reduced sample are provided in Supplemental Material [11].

We performed hard x-ray diffraction measurements at Cornell High Energy Synchrotron Source using a photon energy of 27.3 keV. High energy data at 56.7 keV and additional data from the Advanced Photon Source with a photon energy of 87.4 keV are shown in Supplemental Material [11]. We used a transmission geometry for these measurements with a single-photon counting detector suited for high-energy diffraction. We glued the samples onto Kapton capillaries and cooled them by a helium or nitrogen gas jet. At each temperature, we swept the sample through a full rotation to obtain three dimensional momentum mappings [30].

$1T$-$TiSe_2$ is a layered van der Waals material with an octahedrally coordinated structure [10]. Upon cooling below the transition temperature ($T_{\mathrm{CDW}} = 195$ K in the semimetallic sample), $1T$-$TiSe_2$ undergoes a second-order phase transition into a commensurate $2 \times 2 \times 2$ CDW superstructure. The microscopic driving mechanism giving rise to the CDW order has been controversial for decades, though the emerging consensus is that both excitonic and electron-phonon effects contribute [10,26,31–34]. Regardless, triple-q long-range charge order forms, with the three CDW wave vectors pointing 120° apart when projected onto the plane [Figs. 1(d)–1(g)].

In Fig. 1(a) we show that CDW satellite peaks form below $T_{\mathrm{CDW}} = 195$ K. Three distinct CDW components q_1, q_2, and q_3 are observed at the boundaries of the normal state Brillouin zone [labeled in Fig. 1(b)]. Warming the sample above the transition temperature to 240 K, diffuse scattering near the CDW wave vectors is the dominant feature, as reported previously from a single one-dimensional linecut along (1, K, 3.5) [35]. The diffuse scattering intensity is at least an order of magnitude weaker

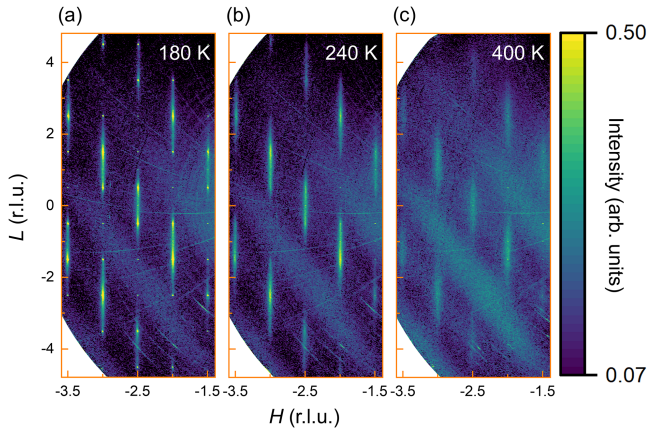

FIG. 2. (H, L) momentum maps at $K = 0.5$ r.l.u. showing sharp CDW diffraction peaks and diffuse scattering arising from CDW fluctuations. (a) At 180 K [$< T_{\mathrm{CDW}}(=195\ \mathrm{K})$], the observed pattern shows sharp peaks, indicative of long-range CDW order. (b) Above T_{CDW}, at 240 K, only diffuse scattering in the form of a raindroplike pattern is clearly visible which indicates the presence of significant interlayer phase fluctuations (CDW stacking faults). (c) Well above T_{CDW} at 400 K, structures within the "raindrops" have disappeared and featureless "rods" remain, which indicates the loss of all out-of-plane phase coherence. The intensity modulation with roughly period four visible in all panels is due to a geometric structure factor. The $K = 0.5$ reciprocal lattice units (r.l.u.) momentum cut is shown schematically in Fig. 1(a) with respect to the in-plane elliptical diffuse scattering. The scale bar is in arbitrary units and follows a logarithmic scale.

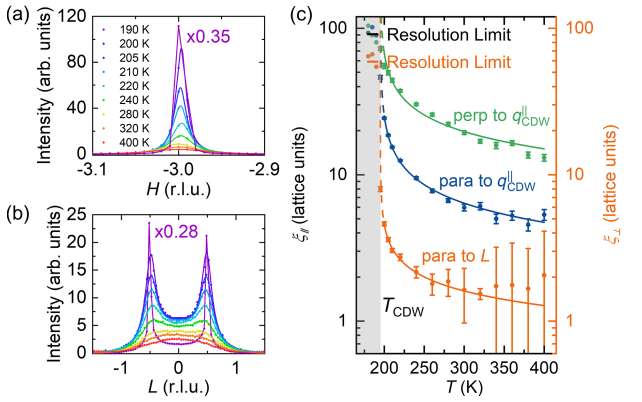

FIG. 3. Momentum scans and correlation lengths at different temperatures. (a) In-plane momentum scans for $(-3.0, 1.5, 0.5)$ along H below and above $T_{\mathrm{CDW}}(=195\ \mathrm{K})$. The constant background far away from the CDW peak is subtracted. Below T_{CDW}, the resolution-limited sharp peak indicates the presence of long-range order, with the line serving as a guide to the eye. Above T_{CDW}, the peaks are fitted with Lorentzians, indicating fluctuating short-range order. (b) Out-of-plane momentum scans for $(-3.0, 1.5, \pm 0.5)$ along L. The scattering profile is fitted with two Lorentzian functions near $L = \pm 0.5$ r.l.u. and a Gaussian function around $L = 0$. (c) Hierarchy of correlation lengths. In-plane and out-of-plane correlation lengths for $(-3.0, 1.5, 0.5)$ are shown. Here, $q^{\parallel}_{\mathrm{CDW}}$ denotes the in-plane CDW wave vector. Solid lines represent fits to power-law dependence of the correlation length on $T - T_{\mathrm{CDW}}$ above T_{CDW}. Below T_{CDW}, in the shaded gray region, the peak width corresponding to long-range order is limited by the instrument resolution. The dashed line represents an extension of the power-law fit to T_{CDW}, showing the diverging behavior. Below T_{CDW}, the correlation lengths are obtained from Gaussian fits to the peaks, while above T_{CDW}, they are extracted from Lorentzian fits.

than the CDW peak intensities at 180 K. As can clearly be seen in Figs. 1(b) and 1(c), the diffuse scattering is anisotropic in the plane. For each of the three CDW peaks, the widths along the major axis of the ellipse are roughly three times those along the minor axis at 240 K. These ellipses effectively become streaks at 400 K, the highest temperature measured in our Letter [Fig. 1(c)]. Importantly, the ellipses for each scattering peak form with their major axes in the direction parallel to the corresponding in-plane CDW wave vector. The orientation of these ellipses implies that the Ti and Se atoms involved in individual CDW components form chainlike structures transverse to each in-plane CDW wave vector, with interchain coupling weaker than the intrachain coupling [Figs. 1(d)–1(g)] [36,37]. These observations are consistent with the proposed hierarchy of energy scales in $1T$-$TiSe_2$ [26].

To visualize the out-of-plane diffuse scattering, we examine (H, L) momentum maps with $K = 0.5$ r.l.u. (reciprocal lattice units) as shown in Fig. 2. The white dashed line drawn in Fig. 1(a) schematically depicts this cut with respect to the in-plane ellipses. Below the CDW transition temperature ($T = 180$ K), the observed peaks in the $K = 0.5$ r.l.u. plane arise due to the CDW superlattice [Fig. 2(a)]. They are resolution limited both in the in-plane and out-of-plane directions, as can be seen more quantitatively in Fig. 3. (Data well below T_{CDW} are presented in Supplemental Material [11]). CDW peaks sit at half-integer L values which indicates that the phase of the charge ordering pattern alternates between adjacent layers.

As the temperature is increased above T_{CDW}, only CDW fluctuations in the form of diffuse scattering is observed. Specifically, scattering intensity from CDW fluctuations form in a "raindroplike" pattern and sharp CDW peaks are no longer present. (The diffuse scattering streaking diagonally across the images are due to thermal diffuse scattering from a transverse acoustic phonon that is not relevant to the present Letter.) For fixed H, intensities of the "raindrop" features are modulated with a period of four reciprocal lattice units along L. These intensity modulations, both in the diffuse scattering and in the CDW peaks below T_{CDW}, arise from the geometric structure factor associated with scattering from the Se atoms. Because the Se planes are positioned roughly $1/4$ and $3/4$ along the c axis in the conventional unit cell, scattering intensities correspondingly vary along L, spanning a period of roughly four reciprocal lattice units. The data can be thought of as complete rods along L that are interrupted by this structure

factor effect. We can thus interpret the rodlike scattering along L as indicating that the CDW fluctuations become uncorrelated in the out-of-plane direction for $T \gg T_{\mathrm{CDW}}$, similar to the recent observation in $1T$-TaS_2 upon photoexcitation [38].

To better quantify the CDW correlation lengths, we take H and L cuts at different temperatures. In Fig. 3(a) we show an H cut of a q_3-type CDW peak with Miller indices (−3.0, 1.5, 0.5). At each temperature a constant background, arising from thermal diffuse scattering from phonons not relevant to the CDW, is subtracted from these cuts. At 190 K, the CDW peak is resolution limited. Above T_{CDW}, the diffuse scattering intensity decreases and the features broaden with increasing temperature. However, even up to our highest measured temperature, $T = 400$ K, diffuse scattering can still be resolved.

Out-of-plane momentum cuts of a pair of q_3-type CDW peaks (−3.0, 1.5, ±0.5) are shown in Fig. 3(b). The CDW peaks at 190 K are resolution limited but have tails arising from diffuse scattering (data well below T_{CDW} showing negligible residual intensity between CDW peaks are presented in Supplemental Material [11]). Above T_{CDW}, the diffuse peaks broaden with increasing temperature, with weight primarily concentrated into a central plateau that constitutes the raindrop centered at $L = 0$ (see Supplemental Material [11]). This raindrop implies that the CDW loses out-of-plane phase coherence, even though the in-plane diffuse scattering indicates that the order within layers remains phase coherent over a considerable length [39–43]. At 280 K, for example, the diffuse scattering possesses a width of $\delta H = 0.05$ r.l.u., but is broad in the L direction with width $\delta L > 1$ r.l.u. [see Figs. 3(a) and 3(b)].

To quantify the anisotropy in the fluctuation regime, we summarize the hierarchy of correlation length scales in Fig. 3(c). In this figure, we plot the in-plane and out-of-plane correlation lengths of a q_3-type CDW peak (−3.0, 1.5, 0.5) as a function of temperature above T_{CDW}. The fluctuations of each CDW component are clearly anisotropic in the plane, with the longer (shorter) correlation lengths in the direction perpendicular (parallel) to the in-plane wave vector of the corresponding CDW component. Meanwhile, the out-of-plane fluctuations have much shorter correlation lengths than in-plane ones above T_{CDW}. At 280 K, the CDW order in real space is everywhere locally triple q in nature, but each CDW component contains domain walls across which the CDW modulation pattern is inverted (i.e., undergoes π phase slip). The characteristic length scale between such domain walls is about 22 unit cells perpendicular to the in-plane wave vector of the CDW component, 7 unit cells parallel to the in-plane wave vector, and 2 unit cell in the out-of-plane direction [Fig. 3(c)]. This anisotropy is inherent within each individual CDW component, such that global threefold rotational symmetry is preserved by the combination of

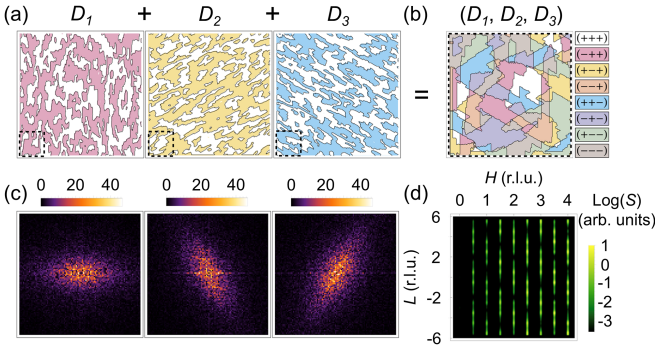

FIG. 4. Structure factors from real space anisotropic CDW fluctuations. Because the charge order in $1T$-$TiSe_2$ occurs in the strong coupling regime, the CDW amplitude is expected to be nonzero throughout the sample well above T_{CDW}. Finite correlation lengths in individual CDW components originate in domain walls across which individual CDW components invert (equivalent to a π phase slip consistent with the $2 \times 2 \times 2$ order). (a) In-plane domain distributions for the three CDW components obtained from modeling domains by an anisotropic Ising model (see Supplemental Material for details [11]). (b) Overlapping the smaller dashed windows marked in the three plots in (a) yields the overall CDW distribution, with eight types of domains. (c) Simulated diffuse scattering from CDW fluctuations at each of the three in-plane CDW vectors q_i, obtained by Fourier transforming the corresponding plot in (a) and enlarging around the origin. The anisotropy in the scattering intensity reproduces the experimental observations shown in Fig. 1(b). (d) Simulated (H, L) structure factor for $K = 0.5$ r.l.u., in the presence of a random stacking of alternating types of domains (see Supplemental Material for details [11]). The intensity modulations of the "rods" reproduce the observed modulations shown in Fig. 2(c).

three CDW components in the overall fluctuating triple-q CDW order, as schematically depicted in Figs. 4(a) and 4(b). Note that the correlation lengths along both in-plane and out-of-plane directions can be seen to all diverge at the same critical temperature T_{CDW} by fitting their temperature dependence above T_{CDW} to power laws in $T - T_{\mathrm{CDW}}$, as shown in Fig. 3 (see Supplemental Material for details [11]).

The simple picture that emerges from our studies is captured in Fig. 4. Similar to most CDW-forming transition metal dichalcogenides, $1T$-$TiSe_2$ lies in the strong coupling limit with $2\Delta(0)/k_B T_{\mathrm{CDW}} \approx 8.7$ [23]. It is expected, therefore, that a nonzero CDW amplitude is present throughout the sample in the temperature regime $T_{\mathrm{CDW}} \lesssim T \ll T_{\mathrm{MF}} \approx 500$ K, without it being phase coherent over long distances [24,25]. The correlation lengths of each CDW component are determined by the mean distance between phase slips. These phase slips are dynamic so that neither short- nor long-range static order is present above T_{CDW}, except in regions near impurities, which can pin CDW order [44,45]. Because the phase slips occur independently for individual CDW components (see Supplemental Material [11]), neighboring, fluctuating triple-q regions in real space typically differ by a π phase flip of just one component. Combining three CDW

components, a total of eight different triple-q fluctuation domain types can form. Many such domains together [Fig. 4(b)] result in the anisotropic diffuse scattering intensities shown in Fig. 4(c), which reproduces the experimental observation in Fig. 1. Similarly, Fig. 4(d) shows calculated structure factors in the (H, L) plane in the presence of randomly stacked, but in-plane-coherent CDWs (see Supplemental Material for details [11]), which reproduces the raindrop pattern of Fig. 2.

Our results illustrate how a simple 2D-to-3D crossover picture is inadequate in describing the emergence of long-range order from local fluctuations in $1T$-$TiSe_2$. The picture of anisotropic CDW fluctuations presented here may generalize to many other systems. The transition is instead characterized by anisotropic domains within each CDW component. A hierarchy of length scales combines to yield a highly structured pattern of fluctuations upon approaching the transition temperature, as predicted in Ref. [26]. Importantly, the fluctuations persist to high temperatures, and may therefore play an important role in the thermodynamic and electronic properties of these materials.

Acknowledgments—We thank Doug Robinson for help with our x-ray diffraction measurements. X-ray experiments were supported by the U.S. Department of Energy, Office of Basic Energy Sciences Grant No. DE-FG02-06ER46285 (P. A.) and Grant No. DE-SC0023017 (A. K.). F. F. acknowledges support from the Engineering and Physical Sciences Research Council, Grant No. EP/X012239/1. F. J. acknowledges support from Grant No. PID2021-128760NB0-I00 from the Spanish MCIN/AEI/10.13039/501100011033/FEDER, European Union. P. A. acknowledges the Gordon and Betty Moore Foundation EPiQS Initiative through Grant No. GBMF9452. Research at the University of Maryland was supported by the Gordon and Betty Moore Foundation's EPiQS Initiative through Grant No. GBMF9071, the U.S. National Science Foundation (NSF) Grant No. DMR2303090, and the Maryland Quantum Materials Center. T. C. C. is supported by the U.S. Department of Energy (DOE), Office of Science (OS), Office of Basic Energy Sciences, Division of Materials Science and Engineering, under Grant No. DE-FG02-07ER46383. G. K. acknowledges support by the National Science Foundation under Grant No. ECCS-1711015. Work at Argonne (M. J. K., S. R., R. O.: data collection and reduction) was supported by the U.S. Department of Energy, Office of Science, Basic Energy Sciences, Materials Sciences and Engineering Division. Use of the Advanced Photon Source at Argonne National Laboratory was supported by the U.S. Department of Energy, Office of Science, Office of Basic Energy Sciences under Contract No. DE-AC02-06CH11357.

Data availability—The data that support the findings of this Letter are openly available [46].

[1] N. Goldenfeld, *Lectures on Phase Transitions and the Renormalization Group* (CRC Press, Boca Raton, 2018).
[2] M. Collins, *Magnetic Critical Scattering* (Oxford University Press, New York, 1989), Vol. 4.
[3] J. G. Donath, F. Steglich, E. D. Bauer, J. L. Sarrao, and P. Gegenwart, Phys. Rev. Lett. **100**, 136401 (2008).
[4] K. Hirakawa, J. Appl. Phys. **53**, 1893 (1982).
[5] A. Ron, E. Zoghlin, L. Balents, S. Wilson, and D. Hsieh, Nat. Commun. **10**, 1654 (2019).
[6] T. Valla, P. Johnson, Z. Yusof, B. Wells, Q. Li, S. Loureiro, R. Cava, M. Mikami, Y. Mori, M. Yoshimura *et al.*, Nature (London) **417**, 627 (2002).
[7] A. R. Wildes, H. M. Rønnow, B. Roessli, M. J. Harris, and K. W. Godfrey, Phys. Rev. B **74**, 094422 (2006).
[8] A. R. Wildes, V. Simonet, E. Ressouche, G. J. McIntyre, M. Avdeev, E. Suard, S. A. J. Kimber, D. Lançon, G. Pepe, B. Moubaraki *et al.*, Phys. Rev. B **92**, 224408 (2015).
[9] J. A. Wilson, F. Di Salvo, and S. Mahajan, Adv. Phys. **24**, 117 (1975).
[10] K. Rossnagel, J. Phys. Condens. Matter **23**, 213001 (2011).
[11] See Supplemental Material at http://link.aps.org/supplemental/10.1103/j8vm-wb65 for details of the theory, which includes Refs. [12–21].
[12] J. van Wezel, Europhys. Lett. **96**, 67011 (2011).
[13] S.-Y. Xu, Q. Ma, Y. Gao, A. Kogar, A. Zong, A. M. M. Valdivia, T. H. Dinh, S.-M. Huang, B. Singh, C.-H. Hsu *et al.*, Nature (London) **578**, 545 (2020).
[14] Y. Peng, X. Guo, Q. Xiao, Q. Li, J. Strempfer, Y. Choi, D. Yan, H. Luo, Y. Huang, S. Jia *et al.*, Phys. Rev. Res. **4**, 033053 (2022).
[15] F. J. Di Salvo, D. E. Moncton, and J. V. Waszczak, Phys. Rev. B **14**, 4321 (1976).
[16] W. L. McMillan, Phys. Rev. B **16**, 643 (1977).
[17] M. Cazzaniga, H. Cercellier, M. Holzmann, C. Monney, P. Aebi, G. Onida, and V. Olevano, Phys. Rev. B **85**, 195111 (2012).
[18] S. V. Borisenko, A. A. Kordyuk, V. B. Zabolotnyy, D. S. Inosov, D. Evtushinsky, B. Büchner, A. N. Yaresko, A. Varykhalov, R. Follath, W. Eberhardt *et al.*, Phys. Rev. Lett. **102**, 166402 (2009).
[19] Y. Feng, J. van Wezel, J. Wang, F. Flicker, D. M. Silevitch, P. B. Littlewood, and T. F. Rosenbaum, Nat. Phys. **11**, 865 (2015).
[20] J.-P. Castellan, S. Rosenkranz, R. Osborn, Q. Li, K. E. Gray, X. Luo, U. Welp, G. Karapetrov, J. P. C. Ruff, and J. van Wezel, Phys. Rev. Lett. **110**, 196404 (2013).
[21] R. Bianco, M. Calandra, and F. Mauri, Phys. Rev. B **92**, 094107 (2015).
[22] W. L. McMillan, Phys. Rev. B **12**, 1187 (1975).
[23] G. Li, W. Z. Hu, D. Qian, D. Hsieh, M. Z. Hasan, E. Morosan, R. J. Cava, and N. L. Wang, Phys. Rev. Lett. **99**, 027404 (2007).
[24] F. Flicker and J. van Wezel, Nat. Commun. **6**, 7034 (2015).
[25] F. Flicker and J. van Wezel, Phys. Rev. B **94**, 235135 (2016).
[26] J. van Wezel, P. Nahai-Williamson, and S. S. Saxena, Phys. Rev. B **81**, 165109 (2010).
[27] D. J. Campbell, C. Eckberg, P. Y. Zavalij, H.-H. Kung, E. Razzoli, M. Michiardi, C. Jozwiak, A. Bostwick, E. Rotenberg, A. Damascelli *et al.*, Phys. Rev. Mater. **3**, 053402 (2019).

[28] M. Iavarone, R. Di Capua, X. Zhang, M. Golalikhani, S. A. Moore, and G. Karapetrov, Phys. Rev. B **85**, 155103 (2012).
[29] P. Husaníková, J. Fedor, J. Dérer, J. Šoltýs, V. Cambel, M. Iavarone, S. J. May, and G. Karapetrov, Phys. Rev. B **88**, 174501 (2013).
[30] M. J. Krogstad, S. Rosenkranz, J. M. Wozniak, G. Jennings, J. P. Ruff, J. T. Vaughey, and R. Osborn, Nat. Mater. **19**, 63 (2020).
[31] A. Kogar, M. S. Rak, S. Vig, A. A. Husain, F. Flicker, Y. I. Joe, L. Venema, G. J. MacDougall, T. C. Chiang, E. Fradkin *et al.*, Science **358**, 1314 (2017).
[32] H. Cercellier, C. Monney, F. Clerc, C. Battaglia, L. Despont, M. G. Garnier, H. Beck, P. Aebi, L. Patthey, H. Berger *et al.*, Phys. Rev. Lett. **99**, 146403 (2007).
[33] M. Porer, U. Leierseder, J.-M. Ménard, H. Dachraoui, L. Mouchliadis, I. Perakis, U. Heinzmann, J. Demsar, K. Rossnagel, and R. Huber, Nat. Mater. **13**, 857 (2014).
[34] M. Burian, M. Porer, J. R. L. Mardegan, V. Esposito, S. Parchenko, B. Burganov, N. Gurung, M. Ramakrishnan, V. Scagnoli, H. Ueda *et al.*, Phys. Rev. Res. **3**, 013128 (2021).
[35] M. Holt, P. Zschack, H. Hong, M. Y. Chou, and T.-C. Chiang, Phys. Rev. Lett. **86**, 3799 (2001).
[36] Y. Cheng, A. Zong, J. Li, W. Xia, S. Duan, W. Zhao, Y. Li, F. Qi, J. Wu, L. Zhao *et al.*, Nat. Commun. **13**, 963 (2022).
[37] Y. Cheng, A. Zong, L. Wu, Q. Meng, W. Xia, F. Qi, P. Zhu, X. Zou, T. Jiang, Y. Guo *et al.*, Nat. Phys. **20**, 54 (2024).
[38] T. Domröse, T. Danz, S. F. Schaible, K. Rossnagel, S. V. Yalunin, and C. Ropers, Nat. Mater. **22**, 1345 (2023).
[39] R. Amin, J. Pandey, K. Beyer, and V. Petkov, Phys. Rev. B **109**, 144106 (2024).
[40] P. Chen, Y.-H. Chan, X.-Y. Fang, Y. Zhang, M.-Y. Chou, S.-K. Mo, Z. Hussain, A.-V. Fedorov, and T.-C. Chiang, Nat. Commun. **6**, 8943 (2015).
[41] P. Chen, Y.-H. Chan, X.-Y. Fang, S.-K. Mo, Z. Hussain, A.-V. Fedorov, M. Chou, and T.-C. Chiang, Sci. Rep. **6**, 37910 (2016).
[42] X.-Y. Fang, H. Hong, P. Chen, and T.-C. Chiang, Phys. Rev. B **95**, 201409(R) (2017).
[43] K. Woo, F. Brown, W. McMillan, R. Miller, M. Schaffman, and M. Sears, Phys. Rev. B **14**, 3242 (1976).
[44] C. J. Arguello, S. P. Chockalingam, E. P. Rosenthal, L. Zhao, C. Gutiérrez, J. H. Kang, W. C. Chung, R. M. Fernandes, S. Jia, A. J. Millis *et al.*, Phys. Rev. B **89**, 235115 (2014).
[45] U. Chatterjee, J. Zhao, M. Iavarone, R. Di Capua, J. Castellan, G. Karapetrov, C. Malliakas, M. G. Kanatzidis, H. Claus, J. Ruff *et al.*, Nat. Commun. **6**, 6313 (2015).
[46] X. Guo, A. Kogar, J. Henke, F. Flicker, F. de Juan, S. X.-L. Sun, I. Khayr, Y. Peng, S. Lee, M. J. Krogstad *et al.*, 10.5281/zenodo.16914816 (2025).